IEEE Access
Multidisciplinary | Rapid Review | Open Access Journal

Received March 17, 2020, accepted March 31, 2020, date of publication April 6, 2020, date of current version April 21, 2020.

Digital Object Identifier 10.1109/ACCESS.2020.2985750

Hydrophilic Direct Bonding of MgO/MgO for High-Temperature MEMS Devices

JIA LIU, PINGGANG JIA, (Senior Member, IEEE), JIASHUN LI, FEI FENG, TING LIANG, WENYI LIU, AND JIJUN XIONG

Science and Technology on Electronic Test and Measurement Laboratory, North University of China, Taiyuan 030051, China

Corresponding author: Jijun Xiong (xiongjijun@nuc.edu.cn)

This work was supported in part by the National Natural Science Foundation of China under Grant 51935011, in part by the Innovative Research Group Project of National Science Foundation of China under Grant 51821003, and in part by the Fund for Shanxi 1331 Project Key Subject Construction.

ABSTRACT Single-crystalline magnesium oxide (MgO) is an attractive material of substrates for high-temperature devices and high-temperature superconducting films. However, it is difficult to achieve the direct bonding of MgO/MgO because of its high brittleness and hardness, as well as the weak bonding force between the crystal faces. In this paper, we presented a hydrophilic direct bonding method of MgO by using two-step surface activation and a high-temperature annealing process. The bonding strengths under different annealing temperatures, pressures and times were measured. A high bonding strength (~7 MPa) and a fine bonding interface without any microcracks and voids were obtained after annealing at 1200 °C, 140 min and 4 MPa. The bonding interface was characterized by scanning electron microscopy (SEM) and transmission electron microscopy (TEM). The bonding mechanism of MgO/MgO was also clearly clarified. For the demo application, a MgO sealed cavity was formed by using the direct bonding method which is commonly used in the microelectromechanical systems (MEMS) devices for harsh environment applications.

INDEX TERMS MgO single crystal, direct bonding, surface activation, high temperature annealing, bonding interface.

I. INTRODUCTION

Single-crystalline magnesium oxide (MgO) is an attractive alternate material to sapphire and silicon for microelectromechanical systems (MEMS) applications because of its superior mechanical and thermal properties at elevated temperatures [1]–[3]. Features of MgO, such as low dielectric constant (≤9.6), low high-frequency dielectric loss, ultra-high melting point (2800 °), and good lattice matching with high-temperature superconducting materials all support it as strong candidate substrates for the fabrication of high-temperature sensors in some areas (e.g. gas turbines, combustors, and other aerospace propulsion applications, etc.) [4]–[6]. Since the wafer bonding is a fundamental technology of MEMS, the direct bonding of MgO plays an important role in MgO-based sensor manufacturing [7]–[11]. However, MgO is an ionic crystal with high hardness and brittleness, and the bonding force between the crystal faces is very weak.

The associate editor coordinating the review of this manuscript and approving it for publication was Hassen Ouakad.

Plasma-activated bonding is one of the promising facile methods in hydrophilic bonding field. To date, $Ar/O_2/N_2$ plasma activation has been successfully applied to the direct bonding of SiO_2 and glass [12], [13]. Wang *et al.* proposed a method to reduce voids formation between the bonding interfaces of Si-based materials by using O_2 plasma activation with fluorine [14]–[16]. Currently, on the basis of successful application of vacuum ultraviolet (VUV) in Au/Au direct bonding and polyether ether ketone (PEEK) and Pt heterogeneous bonding [17], [18]. Xu *et al.* used VUV/O_3 activation and a multistep low-temperature annealing process to achieve the direct bonding of Si/quartz glass, Si/Si, quartz/quartz and SiC to some other materials (eg. SiO_2 and glass) and enhance their bonding strength [19]–[22]. Li *et al.* proposed a hydrophilic sapphire wafer bonding method by combining O_2 plasma activation and high temperature bonding process, which have been successfully applied in wireless passive sensors and fiber-optic pressure sensors for harsh environments [23]–[26]. Silke H. Christiansen *et al.* also enhanced the bonding energy of wafers via high temperature annealing process [27], [28]. These reports demonstrate the importance

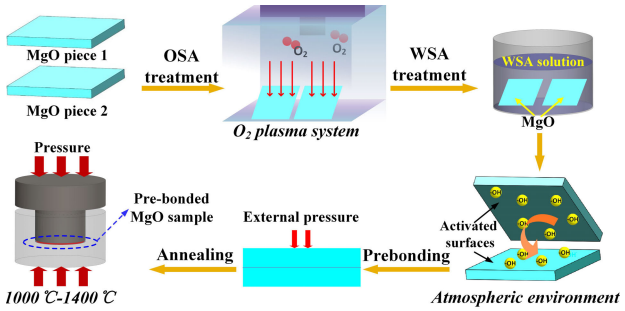

FIGURE 1. Schematic of MgO direct bonding process.

of O_2 plasma activation and high temperature annealing in the fields of single crystal oxides bonding. Moreover, to avoid the damage of temperature-sensitive components and broaden doping profile, wet surface chemical activation was introduced to achieve wafer pre-bonding and reduce the annealing temperature [29]–[31].

Recently, many researchers have focused on the homogenous bonding (eg. Si/Si, quartz/quartz, sapphire/sapphire, and so on) and heterogeneous bonding (eg. Ge/Si [32], [33], Glass/$LiNbO_3$ [34], GaAs/GaN [35]) instead of MgO/MgO, and the bonding mechanism has never been explored. In this paper, a hydrophilic direct bonding method of MgO/MgO that assisted by a two-step surface activation and then high-temperature annealing process was proposed for the first time. After activation treatments, the MgO surface was characterized by atomic force microscope (AFM) and water contact angle (CA). The bonding strength under different annealing conditions was measured by a tensile tester to optimize the bonding parameters. To gain insight into the bonding mechanism, the bonding interface was investigated by the scanning electron microscope (SEM) and the transmission electron microscopy (TEM). Besides, a MgO bonded structure with well-sealed cavity was formed by using wet chemical etching and the proposed direct bonding method. The bonding method presented in this paper can achieve high bonding strength of MgO/MgO, which has the potential to be broadly used in the fabrication of high-temperature MEMS devices.

II. EXPERIMENTAL

The direct bonding procedures of the MgO/MgO illustrated in Fig. 1 include four primary steps: oxygen plasma surface activation (OSA), wet chemical surface activation (WSA), pre-bonding, and high-temperature annealing.

A. MEATERIALS AND SAMPLES PREPARATION

{100}-faces, double-polished MgO pieces with a size of 10 mm×10 mm×200 μm were used for direct bonding. The samples were provided by Shanghai Institute of Ceramic, Chinese Academy of Sciences, Shanghai, China. The MgO pieces with the root mean square (RMS) roughness of approximately 0.45 nm were polished by chemical mechanical polishing technique (CMP). Prior to the surface activation, the samples were cleaned by gasoline, alcohol, RCA-1 (NH_4OH: H_2O_2: H_2O = 1:2:7 by volume) solution and deionized (DI) water for several times and then dried with high purity nitrogen (N_2) gas. The cleaning steps are listed in Table 1.

TABLE 1. Cleaning steps and parameters of MgO.

Step	Conditions	Duration (min)	Function
Gasoline	Room temperature	15	Remove the residual wax from polishing
Alcohol	Room temperature	120	Remove ester and gasoline
RCA-1	Water bath (80 °C)	15	Remove organic particles

B. TWO-STEP SURFACE ACVATION PROCEDURE

Two-step surface activation was used to further clean the MgO surface and increase the hanging groups. Specifically, the two MgO pieces were introduced to a plasma system (IoN Wave 10, America) and sputtered by O_2 plasma for OSA processing. The power and chamber pressure are 200 W and 200 mtorr, respectively. The flow rate of O_2 is 200 sccm. Subsequently, the two MgO samples were immediately immersed in WSA solution of NH_4OH: H_2O_2: H_2O (NH_4OH: H_2O_2: H_2O = 1:1:5 by volume). The effects of different durations of two-step surface activation on the surface roughness, the hydrophilicity and the pre-bonding of the MgO samples were investigated.

C. PRE-BONDING PROCEDURE

After two-step surface activation, the two MgO pieces were covered immediately form one of the edges in air. Then, a low force was loaded to the center of the pieces to make them sufficiently contact and achieve the maximum removal of the residual WSA solution. This process is called pre-bonding and accomplished at room temperature in a thousand-level clean room. The pre-bonding strength is very low because of the weak van der Waals force between the pieces. Therefore, the pre-bonded MgO samples were subjected to high-temperature annealing process to enhance the bonding strength. In addition, the implementation of pre-bonding avoids pollution during the transferring to the annealing device and thereby reduces the voids formation.

D. HIGH-TEMPERATURE ANNEALING PROCESS

The pre-bonded MgO samples were transferred to a high temperature hot-press system (Jiangtai Co., Ltd., China) for high-temperature annealing process, as shown in Fig. 2. The system includes an electric control cabinet, a hydraulic pump and a high-temperature hot-press furnace (HTPF). The pre-bonded MgO samples were put in a self-designed graphite mold and then introduced to the HTPF, as shown in Fig. 2(b). The annealing temperature is controlled by the electric-control cabinet, the heating rate of which is

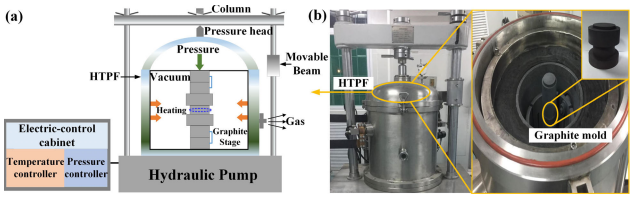

FIGURE 2. The high temperature hot-press system.

modulated by the power. The pressure on MgO was applied by the hydraulic pump and the pressure head displacement control system. Moreover, the bench and the movable beam of the HTPF were equipped with a cylindrical connector to ensure the verticality of the applied pressure during the annealing process.

In addition, the pre-bonded MgO samples were annealed under the different temperatures and pressures for different time to investigate the bonding strength.

E. CHARACTERIZATION

The surface roughness was measured by an AFM (Multimode 8, Bruker, Germany) and expressed by the RMS value. The CA was measured by the contact angle meter DSA 100 (Kruss Co. Ltd., Germany) to clarify the hydrophilicity of the activated-MgO. The bonded MgO sample were glued with the jigs. A tensile test was executed by tensile tester (Instron 2710, England) at a speed of 0.5 mm/min to determine the bonding strength. For the bonding interface characterization, cross sections of the bonded samples were observed through a SEM (SU5000, HITACHI, Japan) and a TEM (Tecnai F20, FEI). EDS analysis attached to SEM and Energy-dispersive X-ray (EDX) analysis coupled with TEM were performed across the bonding interface. Moreover, the bubbles and the voids at the bonding interface were characterized by the C-mode scanning acoustic microscope (C-SAM, Sonoscan D9500, America). The TEM MgO test samples were made using a focusing ion beam (FIB) process.

III. RESULTS AND DISCUSSION

A. SURFACE ROUGHNESS CHARACTERIZATION

The RMS values of the MgO pieces before and after surface activation are listed in Table 2. When the sample was only treated by OSA for a short time, the surface roughness was not significantly changed. However, the RMS value increases slightly with the increasing of the activation time, which may be the surface damaged by the long-term bombardment of high-energy particles. The surface roughness changes significantly with the WSA time, and the samples are not suitable for direct bonding when the activation time exceeds 180 s. In addition, two MgO wafers cannot achieve pre-bonding when only treated by one-step surface activation (OSA and WSA). On the contrast, the two samples A-E after two-step surface activation can achieve pre-bonding and can meet the minimum roughness requirement in MEMS manufacturing. For further analyzing the effect of the two-step activation

TABLE 2. Surface roughness of MgO before and after surface activation.

	Surface treatment		RMS value (nm)		Pre-bonding
Sample	OSA (s)	WSA (s)	Before treatment	After treatment	
	0	60	0.365	0.437	×
	0	120	0.368	0.492	×
	0	180	0.374	0.605	×
	0	240	0.352	0.810	×
	0	300	0.326	0.858	×
	30	0	0.321	0.372	×
	45	0	0.365	0.402	×
	60	0	0.334	0.415	×
	75	0	0.354	0.486	×
	90	0	0.401	0.572	×
A	30	60	0.324	0.421	√
B	30	120	0.347	0.538	√
C	45	60	0.324	0.464	√
D	60	60	0.358	0.504	√
E	75	60	0.358	0.512	√

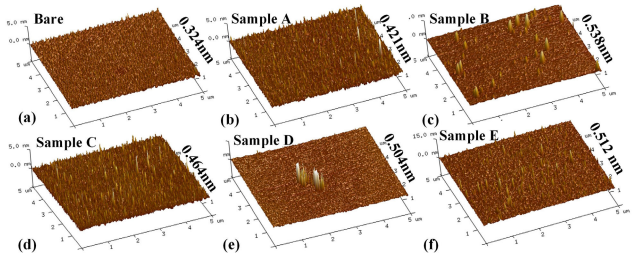

FIGURE 3. 3D AFM images ($5 \times 5\mu$ m^2) of the MgO (a) before and (b)-(f) after two-step surface activation.

treatment on the surfaces, 3D AFM images of samples A-E with area of $5 \times 5\ \mu m^2$ is shown in Fig. 3. The surface roughness morphology of the activated-MgO shows some non-uniform spaced surface irregularities. Some asperities appear on the surface due to the impact of high-energy particles and the erosion of the WSA solution. Moreover, the RMS value of sample A after two-step activation treatment is the smallest (increased from 0.324 nm to 0.421 nm).

B. HYDROPHILICITY CHARACTERIZATION

To verify the bonding mechanism, a water contact angle test was conducted to investigate the effect of surface activation on the hydrophilicity of the samples. One of the important reasons for the poor hydrophilicity of MgO is the existence of the adsorbed organics and the low density of the hydroxyl (-OH) groups. As shown in Fig. 4(a), high hydrophilicity surfaces are formed after O_2 plasma activation. The CA values decrease sharply from 79.8° to 2° with the increasing of the OSA treatment time. This means the organic contaminants are removed and the reactive surfaces are generated. Additionally, because the CA increases with the exposure

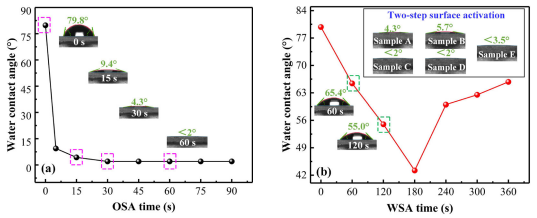

FIGURE 4. Contact angle of MgO versus treatment time of (a) OSA and (b) WSA. The inset shows the CA of samples A-E after two-step surface activation.

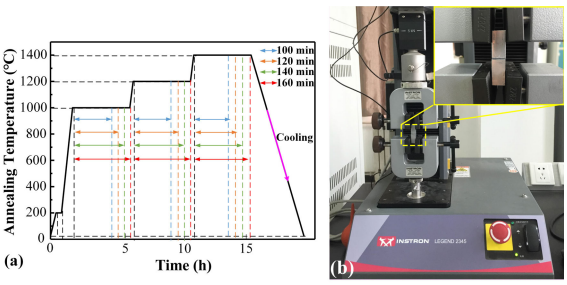

FIGURE 5. (a) Annealing curves of pre-bonded MgO samples at different temperatures and times. (b) Bonding strength measurement platform.

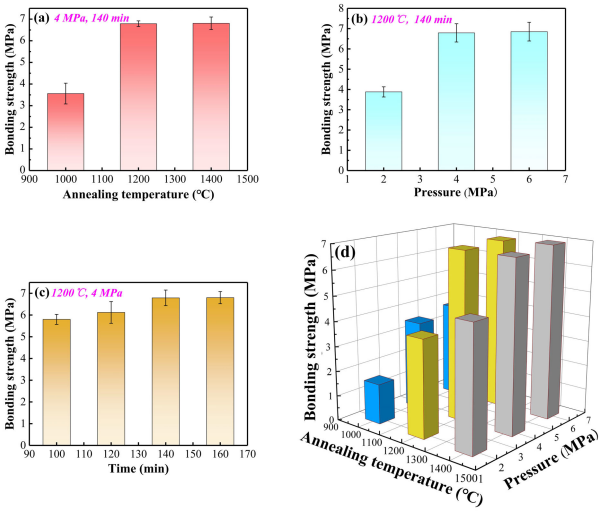

FIGURE 6. Bonding strength of MgO samples under different annealing parameters. The variation of the bonding strength with the (a) annealing temperature, (b) pressure and (c) time. (d) 3D map of the bonding strength under different annealing temperatures and pressures as the annealing time was fixed at 140 min.

time, the MgO samples should be pre-bonded as soon as possible [24]. The result shown in Fig. 4(b) indicates that the use of WSA alone is not an effective way to improve the surface hydrophilicity. However, the WSA solution provides high concentration of OH^-, which helps to achieve pre-bonding of MgO wafers. Subsequently, the CA of MgO samples A-E after two-step surface activation were tested, as shown in the inset of Fig. 4(b). The results illustrate that the two-step surface activation is an effective method to improve surface hydrophilicity and achieve MgO pre-bonding. The durations of OSA and WSA in the two-step activation process were chosen as 30 s and 60 s, respectively.

C. BONDING STRENGTH CHARACTERIZATION

Fig. 5(a) shows the high temperature annealing curve of MgO. Firstly, the pre-bonded MgO samples were heated at 200 °C for 30 min. Then the temperature was raised to 1000 °C, 1200 °C, and 1400 °C with the rate of 10 °C/min, and kept for 100 min, 120 min, 140 min and 160 min, respectively. Meanwhile, different pressures (i.e., 2 MPa, 4 MPa and 6 MPa) were applied to the MgO samples and maintained the same time under the annealing temperature. Finally, the bonded MgO samples were subjected to a tensile test to investigate the effect of the annealing temperatures, times and pressures on the bonding strength, as shown in Fig. 5(b).

As presented in Fig. 6(a), when the annealing time and pressure were fixed at 140 min and 4 MPa, the bonding strength significantly increased to 6.81 MPa with the annealing temperature increasing from 1000 ° to 1200 °. However, the bonding strength did not increase obviously when the annealing temperature exceeding 1200 °. The effect of the pressure on bonding strength was investigated, as shown in Fig. 6(b). A strong bonding strength was obtained under the temperature of 1200 ° and the pressure of ≥ 4 MPa. But the bonded wafers fractured when the pressure exceeded 7 MPa. As shown in Fig. 6(c), when the annealing temperature and pressure were fixed at 1200 ° and 4 MPa, and the annealing time was varied from 100 min to 160 min, the bonding strength was always around 6.78 MPa and did not continue to increase after annealing for 140 min. This means that an annealing time of 140 min is sufficient for atomic interdiffusion across the bonding interface at 1200 °C. For longer annealing time, the bonding interface was stable and the bonding strength kept almost constant. As seen in Fig. 6(d), the bonding strength of the MgO samples after annealing at 1000 ° was weak (<3.5 MPa), which cannot even withstand the mechanical stress produced by SEM sample preparation. Finally, the MgO direct bonding parameters are chosen as a temperature of 1200 °C, a pressure of 4 MPa, and a duration of 140 min.

D. BONDING INTERFACE CHARACTERIZATION

The cross-sectional SEM images of the MgO bonded structures after annealing under the different temperatures at a pressure of 4 MPa is shown in Fig. 7. The SEM samples were separated using laser cutting equipment and splitting pliers. Many cracks and gaps were clearly observed at the bonding interface when the annealing temperature was 1000 °C, as shown in Fig. 7(a). A fine bonding interface without any voids and cracks was obtained when annealing at 1200 °, as shown in Fig. 7(b). Moreover, Figs. 7(c)-(e) show the different magnification SEM images of the bonding interface. It can be seen that the bonding interface is smooth and flat, which indicates that good bonding quality can be achieved when annealing at 1200 °C and 4 MPa.

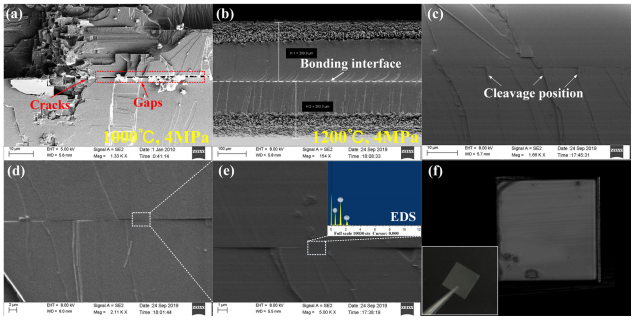

FIGURE 7. Cross-sectional SEM images of the bonded MgO after annealing at (a) 1000 °C and (b) 1200 °C and 4 MPa. Meanwhile, the images at 1.66 kx, 2.11 kx and 5.00 kx magnifications of the bonding interface after annealing at 1200 °C were observed in (c), (d) and (e), respectively. (f) CSAM image of the bonded MgO.

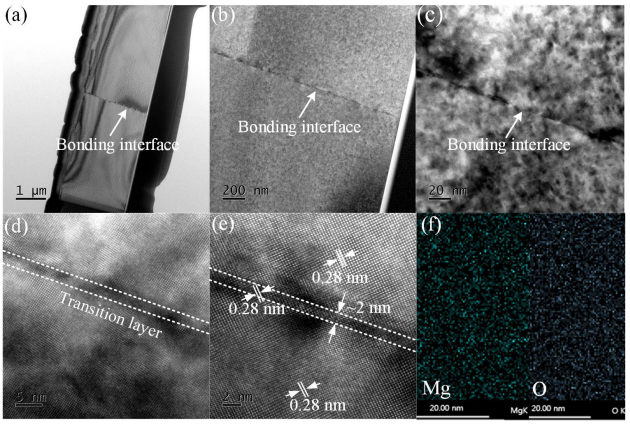

FIGURE 8. TEM images of the MgO bonding interface at (a) 1.99 kx, (b) 10.03 kx, (c) 42.9 kx and (d) 450 kx magnifications. (e) The TEM image at a ultra-high magnification of 1190 kx. (f) EDX mappings: Mg map in dark green and O map in navy blue.

In addition, since the crystal orientations of MgO were not precisely aligned during the pre-bonding process, the cleavage occurred along the crystal orientation. The EDS analysis demonstrates that there were no other elements at the bonding interface except for the existence of the sputtered gold element, as presented in Fig. 7(e). Furthermore, according to the CSAM result shown in Fig. 7(f), few bubbles existed at the edge of the bonded structure, which may be caused by the unevenness of the graphite mold end face.

For gaining insight into the bonding mechanism, a TEM was used to analyze the bonding interface, as shown in Fig. 8. The TEM sample with the size of 2 μm is shown in Fig. 8(a). Figs. 8(b)-(d) show the TEM images of the bonding interface at different magnifications (i.e., ~10 kx, 40 kx and 450 kx) and demonstrate that the bonding interface was void-free and defect-free. As shown in Fig. 8(e), a transition layer of approximately 2 nm was obviously observed across the bonding interface. There was no obvious crystal defects (such as dislocations, lattice defects, and crystal distortion) in the transition layer. Moreover, the distance of the crystal lattices in the transition layer was similar to that at the unbonded places. This means that the connection interface had good crystal quality and was not damaged by high temperature. The EDX mapping illustrated in Fig. 8(f) showed that the Mg and O elemental maps were highlighted in dark green and navy blue, respectively. The results proved that only Mg and O were distributed across the bonding interface layer, which revealed that the interface was not modified.

E. BONDING MECHANISM

The bonding mechanism of MgO was analyzed based on the above results and the bonding model of other materials (sapphire/sapphire and other heterogeneous bonding) [36]–[40], as shown in Fig. 9. The activated-surfaces exhibited high hydrophilicity after OSA process, which means the organic contaminants were easily decomposed and evaporated off, and the density of hydroxyl groups was increased. When the OSA-treated samples immersed in a high -OH concentration solution, the -OH will be filled and adsorbed on the surface, and further increase the number of hydroxyl groups and enhance the surface activation energy. On the other hand, the $Mg(OH)_2$ formed by the diffusion of the water molecules from the air to the surface of MgO (as shown in reaction (1)) is another reason for the increase in -OH. Therefore, the bonded surface after two-step activation will generate a large amount of hydroxyl and Mg-OH groups (as shown in Fig. 9(a)), which are beneficial to the contact area and the pre-bonding strength.

$$MgO + H_2O \rightarrow Mg(OH)_2 \quad (1)$$

Since the hydroxyl groups are easily combined with the water molecules and forms hydrogen bonds, the bonding interface during pre-bonding process is actually contacted by hydrogen bonds between the water molecules and the polar hydroxyl groups, as shown in Fig. 9(b). Since a portion of the residual solution was evaporated along the bonding interface and the Mg-O groups on the sample surfaces were infinitely pulled close, the pre-bonding strength was enhanced [41]. When the pre-bonded sample was annealing at high temperatures, a dehydration condensation reaction (as demonstrated in reaction (2)) occurred on the bonded surfaces. The hydrogen bonds are then converted into high-strength covalent bonds (Mg-O-Mg) [16], [20], as shown in Fig. 9(c). In addition, the small asperities on MgO surface caused by surface activation may have a stronger deformation than the bare MgO, which is beneficial to "dislocation filling" and the closed gaps during the high-temperature annealing process. Meanwhile, the effective contact area between MgO pieces is also increased due to the pressure. This is help to reduce the voids at bonding interface and increase the bonding strength.

$$Mg\text{-}OH + OH\text{-}Mg \rightarrow Mg\text{-}O\text{-}Mg + H_2O \quad (2)$$

In general, the pre-bonding process realizes the preliminary interdiffusion of atoms between the wafers, while the high-temperature annealing facilitates the further interdiffusion of atoms. Finally, a strongly-bonded MgO pair without

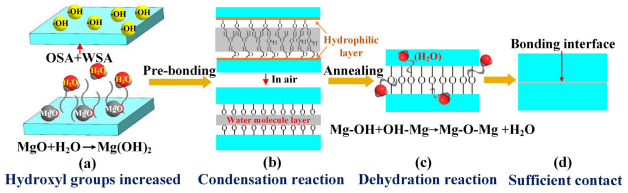

FIGURE 9. Schematic diagrams of MgO bonding mechanism. (a) Two-step surface activation treatment and water molecules absorption, (b) Pre-bonding principle, (c) High-temperature annealing process, (d) Stable bonding interface formation.

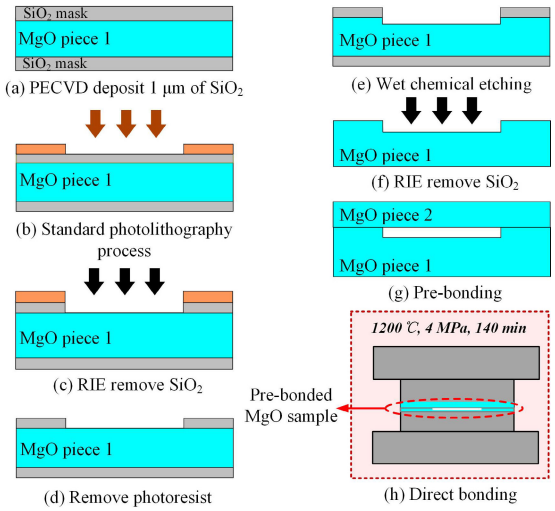

FIGURE 10. Fabrication process of the MgO well-sealed cavity.

voids and deflects is obtained by using hydrophilic direct bonding method, as shown in Fig. 9(d).

F. FABRICATION OF A MGO WELL-SEALED CAVITY

As shown in Figs. 10(a)-(f), a cylindrical cavity was patterned on MgO surface by wet chemical etching method. In our previous work, we have analyzed the effect of different concentrations of etchant on the etching rate and the surface roughness of MgO [42]. Therefore, the parameters of the wet chemical etching process are a phosphoric acid concentration of 50%, a temperature of 120 °, and a duration of 3 min. The cavity was designed with the diameter of 6 mm and the depth of 12 μm on the MgO piece (10 mm×10 mm×0.5 mm). Then, direct bonding of the etched-MgO and a bare MgO (10 mm×10 mm×0.2 mm) under the annealing conditions of 1200 °C, 4 MPa and 140 min to form a sealed cavity. For observing the integrity of the cavity, the bonding interface was tested by SEM, as shown in Fig. 11. The cavity length ($\sim$ 11.54 μm) is consistent with the theoretical etching depth, as shown in Fig. 11(b). This means that there was no obvious collapse and deformation of the cavity after the high temperature bonding procedure. At the same time, the CSAM test result shown in the inset of Fig. 11(a) illustrated a small amount of bubbles around the cavity.

Sealing performance is an crucial indicator to weigh the reliability of the bonding methods and the MEMS devices. Therefore, a leaking experiment was performed on the

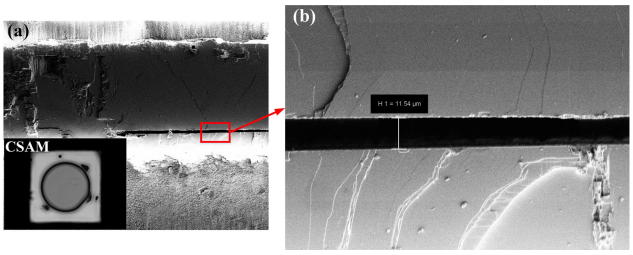

FIGURE 11. The cross-sectional SEM images of the bonding interface of the cavity. Meanwhile, the inset shows the CSAM image of the bonded MgO cavity.

bonded MgO cavity. Firstly, the bonded structure was introduced into an vacuum chamber (<50 Pa) for 30 min. Then the chamber was injected with light fluorine oil and filled with nitrogen to keep the cavity under a pressure of 0.2 MPa for 60 min. The helium leaking rate of the structure is 3.1×10^{-9} Pa·m^3/s, which was less than the limitation of the measured leakage rate of 5×10^{-9} Pa·m^3/s. For further evaluating the sealing of the cavity, the bonded sample was transferred to a heavy fluorinated oil at 125 °C and maintained for 200 min for leaking test. It can be observed that almost no bubbles appeared around the cavity, which indicated that the cavity was well sealed.

IV. CONCLUSION

We proposed a hydrophilic direct bonding method using the two-step surface activation and the high temperature annealing process for a high bonding strength combination of MgO/MgO. A high hydrophilic and reactive surface was formed after the two-step surface activation treatment. The overall surface roughness of the MgO changed a little before and after activation. Moreover, the effect of annealing parameters on bonding strength was investigated, and a high bonding strength of 6.8 MPa was obtained after annealing at 1200 ° and 4 MPa for 140 min. The SEM and TEM images illustrate that the bonding interface was tight and void-free. The transition layer was no crystal defects and dislocations. The leaking test was performed on a bonded MgO cavity to verify the sealing performance of the direct bonding method.

The proposed facile MgO/MgO direct bonding method shows a great potential for developing MgO-based MEMS devices in harsh environment.

REFERENCES

[1] M. Adib, N. Habib, I. Bashter, M. Fathallah, and A. Saleh, "MgO single-crystal as an efficient thermal neutron filter," *Ann. Nucl. Energy*, vol. 38, no. 12, pp. 2673–2679, Dec. 2011.

[2] S. Veldurthi, C.-H. Shin, O.-S. Joo, and K.-D. Jung, "Synthesis of mesoporous MgO single crystals without templates," *Microporous Mesoporous Mater.*, vol. 152, pp. 31–36, Apr. 2012.

[3] D. K. Choge, H.-X. Chen, L. Guo, G.-W. Li, and W.-G. Liang, "Double-pass high-efficiency sum-frequency generation of a broadband orange laser in a single MgO:PPLN crystal," *Opt. Mater. Express*, vol. 9, no. 2, pp. 837–844, Feb. 2019.

[4] D.-S. Gao, X.-D. Gao, Y.-Q. Wu, T.-T. Zhang, J.-N. Yang, and X.-M. Li, "Epitaxial co doped $BaSnO_3$ thin films with tunable optical bandgap on MgO substrate," *Appl. Phys. A, Mater. Sci. Process*, vol. 125, no. 3, Mar. 2019.

[5] A. Aryan, B. Guillet, J. M. Routoure, C. Fur, P. Langlois, and L. Méchin, "Measurement of thermal conductance of $La_{0.7}Sr_{0.3}MnO_3$ thin films deposited on $SrTiO_3$and MgO substrates," *Appl. Surf. Sci.*, vol. 326, pp. 204–210, Jan. 2015.
[6] W. J. Pulliam, P. M. Russler, and R. S. Fielder, "High-temperature high-bandwidth fiber optic MEMS pressure-sensor technology for turbine engine component testing," *Proc. SPIE*, vol. 4578, pp. 229–238, Feb. 2002.
[7] T. Suni, K. Henttinen, I. Suni, and J. Makinen, "Effects of plasma activation on hydrophilic bonding of Si and SiO_2," *J. Electrochem. Soc.*, vol. 149, no. 6, pp. 348–351, 2002.
[8] Z. Liu and D. L. DeVoe, "Micromechanism fabrication using silicon fusion bonding," *Robot. Comput.-Integr. Manuf.*, vol. 17, nos. 1–2, pp. 131–137, Feb. 2001.
[9] A. M. Cetin and B. Bayram, "Diamond-based capacitive micromachined ultrasonic transducers in immersion," *IEEE Trans. Ultrason., Ferroelectr., Freq. Control*, vol. 60, no. 2, pp. 414–420, Feb. 2013.
[10] G.-S. Chung and R. Maboudian, "Bonding characteristics of 3C-SiC wafers with hydrofluoric acid for high-temperature MEMS applications," *Sens. Actuators A, Phys.*, vol. 119, no. 2, pp. 599–604, Apr. 2005.
[11] H. So and D. G. Senesky, "Rapid fabrication and packaging of AlGaN/GaN high-temperature ultraviolet photodetectors using direct wire bonding," *J. Phys. D, Appl. Phys.*, vol. 49, no. 28, Jul. 2016, Art. no. 285109.
[12] A. U. Alam, M. M. R. Howlader, and M. J. Deen, "Oxygen plasma and humidity dependent surface analysis of silicon, silicon dioxide and glass for direct wafer bonding," *ECS J. Solid State Sci. Technol.*, vol. 2, no. 12, pp. P515–P523, 2014.
[13] U. I. Can and B. Bayram, "Plasma-activated direct bonding of patterned silicon-on-insulator wafers to diamond-coated wafers under vacuum," *Diamond Rel. Mater.*, vol. 47, pp. 53–57, Aug. 2014.
[14] C. Wang and T. Suga, "Investigation of fluorine containing plasma activation for room-temperature bonding of Si-based materials," *Microelectron. Rel.*, vol. 52, no. 2, pp. 347–351, Feb. 2012.
[15] C. Wang, Y. Liu, and T. Suga, "A comparative study: Void formation in silicon wafer direct bonding by oxygen plasma activation with and without fluorine," *ECS J. Solid State Sci. Technol.*, vol. 6, no. 1, pp. P7–P13, Dec. 2016.
[16] C. Wang and T. Suga, "Room-temperature direct bonding using fluorine containing plasma activation," *J. Electrochemical Soc.*, vol. 158, no. 5, pp. 525–529, Mar. 2011.
[17] W. Fu, A. Shigetou, S. Shoji, and J. Mizuno, "Low-temperature direct heterogeneous bonding of polyether ether ketone and platinum," *Mater. Sci. Eng., C*, vol. 79, pp. 860–865, Oct. 2017.
[18] A. Okada, S. Shoji, M. Nimura, A. Shigetou, K. Sakuma, and J. Mizuno, "Vacuum ultraviolet irradiation treatment for reducing Gold–Gold bonding temperature," *Mater. Trans.*, vol. 54, no. 11, pp. 2139–2143, Nov. 2013.
[19] J. Xu, C. Wang, T. Wang, Y. Wang, Q. Kang, Y. Liu, and Y. Tian, "Mechanisms for low-temperature direct bonding of Si/Si and quartz/quartz via VUV/O_3 activation," *RSC Adv.*, vol. 8, no. 21, pp. 11528–11535, Mar. 2018.
[20] J. Xu, C. Wang, T. Wang, Y. Liu, and Y. Tian, "Direct bonding of silicon and quartz glass using VUV/O_3 activation and a multistep low-temperature annealing process," *Appl. Surf. Sci.*, vol. 453, pp. 416–422, Sep. 2018.
[21] J. Xu, C. Wang, D. Li, J. Cheng, Y. Wang, C. Hang, and Y. Tian, "Fabrication of SiC/Si, SiC/SiO_2, and SiC/glass heterostructures via VUV/O_3 activated direct bonding at low temperature," *Ceram. Int.*, vol. 45, no. 3, pp. 4094–4098, Feb. 2019.
[22] C. Wang, J. Xu, S. Guo, Q. Kang, Y. Wang, Y. Wang, and Y. Tian, "A facile method for direct bonding of single-crystalline SiC to Si, SiO_2, and glass using VUV irradiation," *Appl. Surf. Sci.*, vol. 471, pp. 196–204, Mar. 2019.
[23] W. Li, T. Liang, Y. Chen, P. Jia, J. Xiong, Y. Hong, C. Lei, Z. Yao, L. Qi, and W. Liu, "Interface characteristics of sapphire direct bonding for high-temperature applications," *Sensors*, vol. 17, no. 9, p. 2080, 2017.
[24] W. Li, T. Liang, W. Liu, C. Lei, Y. Hong, Y. Li, Z. Li, and J. Xiong, "Interface characteristics comparison of sapphire direct and indirect wafer bonded structures by transmission electron microscopy," *Appl. Surf. Sci.*, vol. 494, pp. 566–574, Nov. 2019.
[25] W. Li, T. Liang, W. Liu, P. Jia, Y. Chen, J. Xiong, C. Lei, Y. Hong, and Y. Li, "Wireless passive pressure sensor based on sapphire direct bonding for harsh environments," *Sens. Actuators A, Phys.*, vol. 280, pp. 406–412, Sep. 2018.
[26] W. Li, T. Liang, P. Jia, C. Lei, Y. Hong, Y. Li, Z. Yao, W. Liu, and J. Xiong, "Fiber-optic Fabry–Pérot pressure sensor based on sapphire direct bonding for high-temperature applications," *Appl. Opt.*, vol. 58, no. 7, pp. 1662–1666, Mar. 2019.
[27] S. H. Christiansen, R. Singh, and U. Gosele, "Wafer direct bonding: From advanced substrate engineering to future applications in micro/nanoelectronics," *Proc. IEEE*, vol. 94, no. 12, pp. 2060–2106, Dec. 2006.
[28] M. Shimbo, K. Furukawa, K. Fukuda, and K. Tanzawa, "Silicon-to-silicon direct bonding method," *J. Appl. Phys.*, vol. 60, no. 8, pp. 2987–2989, Oct. 1986.
[29] M. M. R. Howlader, S. Suehara, H. Takagi, T. H. Kim, R. Maeda, and T. Suga, "Room-temperature microfluidics packaging using sequential plasma activation process," *IEEE Trans. Adv. Packag.*, vol. 29, no. 3, pp. 448–456, Aug. 2006.
[30] Q. Tong, G. Cha, R. Gafiteanu, and U. Gosele, "Low temperature wafer direct bonding," *J. Microelectromech. Syst.*, vol. 3, no. 1, pp. 29–35, Mar. 1994.
[31] C. Mai, M. Li, and S. Yang, "Low temperature direct bonding of silica glass via wet chemical surface activation," *RSC Adv.*, vol. 5, no. 53, pp. 42721–42727, May 2015.
[32] S. Ke, Y. Ye, J. Wu, S. Lin, W. Huang, C. Li, and S. Chen, "Interface characteristics and electrical transport of Ge/Si heterojunction fabricated by low-temperature wafer bonding," *J. Phys. D, Appl. Phys.*, vol. 51, no. 26, Jul. 2018, Art. no. 265306.
[33] M. M. R. Howlader, S. Suehara, and T. Suga, "Room temperature wafer level glass/glass bonding," *Sens. Actuators A, Phys.*, vol. 127, no. 1, pp. 31–36, Feb. 2006.
[34] J. Xu, C. Wang, Y. Tian, B. Wu, S. Wang, and H. Zhang, "Glass-on-$LiNbO_3$ heterostructure formed via a two-step plasma activated low-temperature direct bonding method," *Appl. Surf. Sci.*, vol. 459, pp. 621–629, Nov. 2018.
[35] J. Jasinski, Z. Liliental-Weber, S. Estrada, and E. Hu, "Microstructure of GaAs/GaN interfaces produced by direct wafer fusion," *Appl. Phys. Lett.*, vol. 81, no. 17, pp. 3152–3154, Oct. 2002.
[36] C. Wang, E. Higurashi, and T. Suga, "Void-free room-temperature silicon wafer direct bonding using sequential plasma activation," *Jpn. J. Appl. Phys.*, vol. 47, no. 4, pp. 2526–2530, Apr. 2008.
[37] T. Liang, X. Wang, P. Jia, W. Zhang, C. Xue, and J. Xiong, "Fabrication of bonded SiC structure with cavity based on direct bonding process for MEMS device applications," *Microsyst. Technol.*, vol. 23, no. 1, pp. 225–229, Jan. 2017.
[38] S. Keshavarzi, U. Mescheder, and H. Reinecke, "Room temperature Si–Si direct bonding technique using velcro-like surfaces," *J. Microelectromech. Syst.*, vol. 25, no. 2, pp. 371–379, Apr. 2016.
[39] Z. Fan, G. Ji, Y. Jin, Z. Shi, and X. Wang, "Mechanical analysis of the interface bonding state of a TiO_2 film/Si substrate," *Ceram. Int.*, vol. 45, no. 7, pp. 8798–8803, May 2019.
[40] D. Knorr, N. Tran, K. Williams, J. Andzelm, N. Henry, K. Gaskell, J. Lenhart, N. Baril, C. Jaye, D. Fischer, M. Tidrow, and S. Bandara, "Bonding of cysteamine on InAs surfaces," *Appl. Surf. Sci.*, vol. 462, pp. 489–501, Dec. 2018.
[41] T. Plach, K. Hingerl, S. Tollabimazraehno, G. Hesser, V. Dragoi, and M. Wimplinger, "Mechanisms for room temperature direct wafer bonding," *J. Appl. Phys.*, vol. 113, no. 9, Mar. 2013, Art. no. 094905.
[42] J. Liu, P. Jia, X. Chen, T. Liang, H. Liu, W. Liu, and J. Xiong, "Surface characterization of patterning on MgO single crystals using wet chemical etching process to advance MEMS devices," *J. Micromech. Microeng.*, vol. 30, no. 1, Jan. 2020, Art. no. 015001.

JIA LIU received the B.S. degree from the North University of China, Shanxi, China, in 2014, where she is currently pursuing the Ph.D. degree. Her current research interests include the fields of extreme environmental testing and MEMS devices.

PINGGANG JIA (Senior Member, IEEE) received the B.Sc. degree in applied physics from the China University of Mining and Technology, China, in 2006, and the M.Sc. and Ph.D. degrees in instrument science and technology from Chongqing University, China, in 2013. He is currently an Associate Professor with the North University of China, where he is also a Staff with the Micro and Nano Technology Research Center. His research interests include fiber optic sensors, MEMS, laser-based measurement technology, and high-temperature sensors.

JIASHUN LI, photograph and biography not available at the time of publication.

FEI FENG, photograph and biography not available at the time of publication.

TING LIANG, photograph and biography not available at the time of publication.

WENYI LIU, photograph and biography not available at the time of publication.

JIJUN XIONG received the B.Sc. and M.Sc. degrees in electrical engineering from the North University of China, Shanxi, China, in 1993 and 1998, respectively, and the Ph.D. degree in precision instruments and technology from Tsinghua University, Beijing, China, in 2003. His research interest is in the fields of measurement and MEMS.